

Quadrupole Topological Photonic Crystals

Li He¹, Zachariah Addison¹, Eugene J. Mele¹, & Bo Zhen^{1,*}

¹*Department of Physics and Astronomy, University of Pennsylvania, Philadelphia, PA 19104, USA*

Quadrupole topological phases, exhibiting protected boundary states that are themselves topological insulators of lower dimensions, have recently been of great interest. Extensions of these ideas from current tight binding models to continuum theories for realistic materials require the identification of quantized invariants describing the bulk quadrupole order. Here we identify the analog of quadrupole order in Maxwell's equations for a photonic crystal (PhC) and identify quadrupole topological photonic crystals formed through a band inversion process. Unlike prior studies relying on threaded flux, our quadrupole moment is quantized purely by crystalline symmetries, which we confirm using three independent methods: analysis of symmetry eigenvalues, numerical calculations of the nested Wannier bands, and the expectation value of the quadrupole operator. Furthermore, through the bulk-edge correspondence of Wannier bands, we reveal the boundary manifestations of non-trivial quadrupole phases as quantized polarizations at edges and bound states at corners. Finally, we relate the nontrivial corner states to the emergent phenomena of quantized fractional corner charges and a filling anomaly as first predicted in electronic systems. Our work paves the way to further explore higher-order topological phases in nanophotonic systems and our method of inducing quadrupole phase transitions is also applicable to other wave systems, such as electrons, phonons and polaritons.

Symmetries play a pivotal role in understanding and classifying various topological phases of matter¹⁻⁴. In periodic media, systems with different symmetries can admit different classifications characterized by quantized topological invariants. Furthermore, interface states in symmetry-protected topological (SPT) phases can only robustly exist, between two topologically distinct regions, when required bulk symmetries are preserved at the boundaries. In the simplest example of SPT phases, a one-dimensional (1D) Su-Schrieffer-Heeger (SSH) model, the topological invariant — Zak phase⁵ — is only quantized when inversion symmetry is preserved, leading to edge states that are protected by nonzero bulk polarizations. Recently, the concept of polarization, or bulk dipole moment in crystals, has been generalized to include multipole moments, such as quadrupole and octupole moments, leading to the discovery of higher-order topological insulators (HOTIs)⁶⁻¹⁰. In particular, these HOTIs have vanishing dipole densities but nonzero higher order multiple moments, which can be quantized by certain crystalline symmetries, such as reflection and rotation. In contrast to conventional topological insulators (TIs) that support gapless boundary states, HOTIs exhibit protected boundaries that are, themselves, TIs in lower dimensions.

Quadrupole TIs have been demonstrated recently in a few classical systems, ranging from coupled microwave¹¹ and optical resonators¹² to mechanical modes¹³ and electrical circuits^{14,15}, mostly analyzed as lattice models following the tight-binding approximation. In these models, the adopted symmetry required to quantize the quadrupole moment is reflection or four-fold rotation (C_4) with threaded flux, which is incompatible with spatial symmetries. This leads to fundamental challenges to explore quadrupole phases in realistic materials where lattice models are insufficient, due to the lack of means to quantize bulk topological invariants.

Here we find solutions to Maxwell's equations in PhCs that are the electrodynamic analogs to quadrupole topological phases. The proposed topological PhCs have quantized bulk quadrupole moments, which are protected purely by spatial symmetries. In particular, we show it is straightforward to achieve quadrupole phases in systems with broken time-reversal symmetry (T), which has been overlooked in previous studies. We perform numerical simulations on gyromagnetic photonic crystals to analyze the bulk quadrupole topology and the edge manifestations, and all findings can be readily observed at microwave frequencies^{16,17}.

We start by presenting the topological phase transition between a trivial (Fig. 1a, left panel) and a quadrupole PhC (right panel). The PhC consists of gyromagnetic rods in air. The gapless transition point is achieved in a 2×2 super-cell structure with four square rods (middle panel). All rods are identical in shape and are of the same gyromagnetic material of Yttrium Iron Garnet (YIG) with isotropic dielectric permittivity of $\epsilon = 15\epsilon_0$ and inplane permeability $\mu = 14\mu_0$. To break time-reversal symmetry, an external magnetic field is applied along the out-of-plane direction (z), which induces complex-valued off-diagonal terms in the permeability tensor of YIG¹⁸:

$$\bar{\bar{\mu}} = \begin{bmatrix} \mu & i\kappa & 0 \\ -i\kappa & \mu & 0 \\ 0 & 0 & \mu_0 \end{bmatrix} \quad (1)$$

This gyromagnetic response, $\mu_{xy} = \mu_{yx}^* = i\kappa$, breaks T but preserves C_4 and $M_{x(y)}T$. Here $M_{x(y)}$ is mirror reflection that transforms $x(y)$ to $-x(y)$. At the phase transition, all rods are placed at $a/2$ away from their neighbors; the corresponding band structure for TM modes (E_z, H_x, H_y) has two-fold (four-fold) degeneracies at the center (corner) of the folded Brilluion zone Γ (M).

Both degeneracies are lifted when the four rods are simultaneously displaced inward ($d < 0$, left panel) or outward ($d > 0$, right panel) along the diagonal lines of the unit cell. On either side of the transition point, the band structure is fully gapped (shaded in yellow) and supports two topologically distinct phases determined by the displacement d : for the choice of cell in Fig. 1, inward displacements with negative d give rise to trivial phases, while outward displacements with positive d correspond to quadrupole phases.

Next, we present our calculations of the quadrupole topological invariant q_{xy} , using three different approaches, and demonstrate the phase transition between $q_{xy} = 0$ and $q_{xy} = 1/2$ by displacing the dielectric rods. We start by evaluating q_{xy} using the C_4 eigenvalues at high-symmetry \mathbf{k} points of all bands below the gap^{7,19}:

$$e^{i2\pi q_{xy}} = r_4^+(\Gamma)r_4^{+*}(\mathbf{M}) = r_4^-(\Gamma)r_4^{-*}(\mathbf{M}). \quad (2)$$

Here, r_4^+ (r_4^-) is the C_4 eigenvalue of a mode with C_2 eigenvalue $r_2 = +1$ (-1); naturally, $r_4^+ = \pm 1$ and $r_4^- = \pm i$. Accordingly, a quadrupole topological phase transition happens when two pairs of bands switch their C_4 eigenvalues at the same time — a process we call “double-band-inversion”. Specifically, the double-band inversion happens in our system when d changes from negative to positive: through this process, the TM mode at \mathbf{M} with a phase winding of $+2\pi$ in the E_z mode profile ($r_4 = i$, labeled as green) switches position with the one with the winding of -2π ($r_4 = -i$, label in red); meanwhile, the two modes with $r_4 = \pm 1$ at \mathbf{M} also switch positions. On the other hand, all C_4 eigenvalues at Γ remain unchanged. Using Eq. 2, we identify PhCs with $d > 0$ to be topologically nontrivial, with bulk quadrupole invariant $q_{xy} = 1/2$, and PhCs with $d < 0$ to be topologically trivial with $q_{xy} = 0$.

A more comprehensive topological phase diagram of our system is shown in Fig. 1d, determined by displacement d and strength of gyromagnetic response κ . Both quadrupole topological insulators (green) and trivial insulators (orange) are identified, with the super-cell structure ($d = 0$) being the transition in between the two phases (y -axis). Interestingly, Chern insulating phases (purple) are observed at large displacements, consistent with the broken time-reversal symmetry^{18,20}.

To confirm the quadrupole topology of our PhC, we explicit show that its dipole moments are zero ($p_x = p_y = 0$), but its quadrupole moment is non-zero ($q_{xy} = 1/2$). To this end, we perform two separate sets of calculations using two different methods: (1) the nested Wilson loop formulation⁷; (2) and the expectation value of the exponentiated quadrupole operator^{21,22}, and show they reach the same conclusions. Here, we present the nested Wilson loop calculations, leaving the second method in Supplementary Information section III. We start by computing the band structure and mode profiles (E_z) of the TM modes for a particular displacement of dielectric rods $d = a/4 - w/2$ (Fig. 2a, same as the right panel in Fig. 1a). Using these as input, we compute the Wannier bands $\nu_{x,y}$ for the two lowest-energy bands (Supplementary Information section I). The results (Fig. 2a) show that the Wannier bands — $\nu_{x(y)}$ as a function of $k_{y(x)}$ — for the two lowest bands always sum to 0, proving the bulk dipoles are zero: $p_x = p_y = 0$. Meanwhile, as the two Wannier bands are gapped — one between -0.5 and 0 and the other between 0 and 0.5 — the Wannier states can be separated into two sectors, labeled as ν_x^\pm (ν_y^\pm). To confirm the quadrupole topology, we compute the polarizations of the Wannier bands within one sector, $p_y^{\nu_x^-}$ and $p_x^{\nu_y^-}$, using the nested Wilson loop formulation^{7,23}. As shown in Fig. 2b, both Wannier band polarizations are quantized to be $1/2$ — due to the simultaneous preservation of $M_x T$ and $M_y T$ symmetries

(Supplementary Information section II) — which further confirms our PhC has a nonzero bulk quadrupole moment: $q_{xy} = 2p_x^{\nu_y^-} p_y^{\nu_x^-} = 1/2$.

To compare, we repeat the same set of calculations for a different unit cell with a negative displacement of $d = -(a/4 - w/2)$ (Fig. 2c). As shown, the Wannier bands are also gapped and sum to zero, meaning the bulk dipoles $p_{x,y}$ remain zero. However, the nested Wilson loops, $p_y^{\nu_x^-}$ and $p_x^{\nu_y^-}$, are also zero, leading to a trivial quadrupole moment $q_{xy} = 0$. This correspondence between positive (negative) displacements leading to non-trivial (trivial) quadrupole phases is consistent with our preceding conclusions based on C_4 symmetry eigenvalues. Importantly, the non-trivial and trivial PhCs in Fig. 2 can be simply related to each other, by shifting the choice of the unit cell center by $a/2$. This observation leads to an intuitive understanding of the difference in quadrupole moment between the two phases as discussed in Supplementary Information V.

Next, we present the physical consequences of quadrupole topological PhCs at interfaces, originating from the bulk-edge correspondence of the Wannier bands. Following classical electromagnetism, a non-zero bulk quadrupole moment in a finite system is manifested as edge polarizations at its boundaries. Here we study the 1D interfaces between quadrupole (trivial) PhCs and perfect electric conductors (PECs). We find that the non-trivial quadrupole topology indeed leads to a quantized edge polarization along the interface, which is absent for a trivial PhC. Specifically, we consider a strip of 20 unit cells of the quadrupole (trivial) PhC design, which satisfies periodic boundary condition in the x -direction and closed boundary condition in the y -direction, due to the two PECs on top and bottom as shown in Fig. 3a,b. The energy dispersions $\omega(k_x)$ of the

quadrupole and trivial strips (Fig. 3c,d) share the same bulk energy spectra (gray areas) but have different edge dispersions (gray solid lines), due to their different edge terminations. The Wannier centers ν_x are calculated for the two different strips based on their energy dispersions and Bloch mode profiles (Fig. 3e,f). For the topological strip, two additional Wannier states (red circles) are found to emerge outside the Wannier bands (blue) at the middle of the gap (± 0.5), which is protected by the non-trivial bulk quadrupole moment. This can be understood in a similar way as the in-gap edge states in the 1D SSH model with non-trivial bulk polarization. The quantization of the mid-gap Wannier states at ± 0.5 is due to the additional $M_x T$ symmetry in our system (Supplementary Information section II). In comparison, no additional Wannier states are found inside the Wannier gaps for the trivial strip, consistent with the lack of bulk quadrupole moment.

Furthermore, the two mid-gap Wannier states in the topological strip are spatially localized at the top and bottom edges. To demonstrate this, we further study the spatial distribution of Wannier states by calculating the polarization density p_x as a function of position along y (Supplementary Information section VI). In order to choose a definite sign of the polarization, we introduce an infinitesimal perturbation to break the C_2 symmetry of the semi-infinite strip. For the quadrupole PhC, as shown in Fig. 3g, there are nonzero polarization densities developed near the two edges at $y = 0$ and $y = 20a$, and the edge polarizations are quantized to ± 0.5 . In comparison, neither edge nor bulk polarization are observed in the trivial PhC (Fig. 3h).

Finally, we show the physical consequence of quadrupole PhCs as localized 0D corner states, which are the photonic analogs of states responsible for filling anomalies and fractional charges

in an electronic setting²⁴. To this end, we solve the eigenstates in a finite 2D quadrupole PhC enclosed by PECs, with a thin air gap in between (Fig. 4a). The eigenstates are labeled according to their energies, with the lowest-energy state labeled as 1. Aside from delocalized bulk states, four degenerate states — 199 through 202 — are found, with their energies inside the bulk energy gap (Fig. 4b). Their mode profiles (E_z) confirm that these states are spatially localized at the four corners, with one example shown in Fig. 4c. Due to the lack of chiral symmetry in our system, which is generic in the continuum theory expanded around non-zero frequencies, the energy of the four corner states is not pinned at the center of the bulk energy gap²⁵; instead they can be shifted, even immersed into the bulk continuum, by modifying the refractive index at the corners. This renders the appearance of corner states less of an essential signature of quadrupole phases^{9,11}. In fact, corner states are also found in other higher-order topological phases with vanishing bulk quadrupole moments^{23–31}.

Instead, here we illustrate the nontrivial quadrupole nature of our PhC using the filling anomaly, by counting the number of energy eigenstates below and above a given bulk energy gap⁹ (Fig. 4a). Specifically, even though trivial samples may support corner states, they originate from either the top or bottom band alone, leaving $2N^2 - 4n$ states in the bulk continuum (n is an integer). On the other hand, for nontrivial PhCs, the number of states below and above the energy gap are both $2N^2 - 2 = 198$ ($N = 10$ in our case). This indicates the 4 degenerate corner states we observed are “contributed” by both the top and bottom bands together, and thus proves the non-trivial quadrupole topology of our design. As a consequence, for a quadrupole PhC, quantized fractional charges appear at four corners of a finite sized system (Fig. 4d) when calculate the spatial

distribution of the lowest 200 energy states, in a similar vein as the calculations of charge density in electronic systems at “half-filling” (here we have introduced an infinitesimal perturbation to break C_4 symmetry in order to split the four-fold degenerate corner states). Remarkably, these corner charges are shared by two convergent dipoles on the two perpendicular edges, as the magnitude of the corner charges is equal to the edge polarizations. This further confirms these corner charges originate from a non-zero bulk quadrupole moment. We point out that the observed fractional corner charges arise from the fundamental difference in the counting of bulk states⁹, and was recently proposed in electronic systems by Benalcazar *et al.* as a filling anomaly: a mismatch between number of states in an energy band and the number of electrons required for charge neutrality²⁴.

In summary, we present quadrupole topological photonic crystals with truly quantized invariants and the physical consequences at material’s edges and corners. The proposed gyromagnetic PhCs can be readily realized in the microwave regime. Meanwhile, the coexistence of multiple topological phases in our system, both quadrupole TIs and Chern insulators, provides a versatile platform to further demonstrate topological photonic circuits with protected elements immune to disorders in various dimensions. Finally, our findings of inducing quadrupole phase transitions and quantizing quadrupole moments — through crystalline symmetries in conjunction with broken time-reversal symmetry — can also be applied to other wave systems, including electrons, phonons and polaritons.

1. Schnyder, A. P., Ryu, S., Furusaki, A. & Ludwig, A. W. Classification of topological insulators and superconductors in three spatial dimensions. *Physical Review B* **78**, 195125 (2008).

2. Kitaev, A. Periodic table for topological insulators and superconductors. In *AIP conference proceedings*, vol. 1134, 22–30 (AIP, 2009).
3. Ryu, S., Schnyder, A. P., Furusaki, A. & Ludwig, A. W. Topological insulators and superconductors: tenfold way and dimensional hierarchy. *New Journal of Physics* **12**, 065010 (2010).
4. Chiu, C.-K., Teo, J. C., Schnyder, A. P. & Ryu, S. Classification of topological quantum matter with symmetries. *Reviews of Modern Physics* **88**, 035005 (2016).
5. Zak, J. Berrys phase for energy bands in solids. *Physical review letters* **62**, 2747 (1989).
6. Benalcazar, W. A., Bernevig, B. A. & Hughes, T. L. Quantized electric multipole insulators. *Science* **357**, 61–66 (2017).
7. Benalcazar, W. A., Bernevig, B. A. & Hughes, T. L. Electric multipole moments, topological multipole moment pumping, and chiral hinge states in crystalline insulators. *Physical Review B* **96**, 245115 (2017).
8. Schindler, F. *et al.* Higher-order topological insulators. *Science advances* **4**, eaat0346 (2018).
9. Song, Z., Fang, Z. & Fang, C. (d- 2)-dimensional edge states of rotation symmetry protected topological states. *Physical review letters* **119**, 246402 (2017).
10. Langbehn, J., Peng, Y., Trifunovic, L., von Oppen, F. & Brouwer, P. W. Reflection-symmetric second-order topological insulators and superconductors. *Physical review letters* **119**, 246401 (2017).

11. Peterson, C. W., Benalcazar, W. A., Hughes, T. L. & Bahl, G. A quantized microwave quadrupole insulator with topologically protected corner states. *Nature* **555**, 346 (2018).
12. Mittal, S. *et al.* Photonic quadrupole topological phases. *Nature Photonics* **1** (2019).
13. Serra-Garcia, M. *et al.* Observation of a phononic quadrupole topological insulator. *Nature* **555**, 342 (2018).
14. Imhof, S. *et al.* Topoelectrical-circuit realization of topological corner modes. *Nature Physics* **14**, 925 (2018).
15. Serra-Garcia, M., Süsstrunk, R. & Huber, S. D. Observation of quadrupole transitions and edge mode topology in an lc circuit network. *Physical Review B* **99**, 020304 (2019).
16. Wang, Z., Chong, Y., Joannopoulos, J. D. & Soljačić, M. Observation of unidirectional backscattering-immune topological electromagnetic states. *Nature* **461**, 772 (2009).
17. Skirlo, S. A. *et al.* Experimental observation of large chern numbers in photonic crystals. *Physical review letters* **115**, 253901 (2015).
18. Wang, Z., Chong, Y., Joannopoulos, J. D. & Soljačić, M. Reflection-free one-way edge modes in a gyromagnetic photonic crystal. *Physical review letters* **100**, 013905 (2008).
19. Wieder, B. J. *et al.* Strong and” fragile” topological dirac semimetals with higher-order fermi arcs. *arXiv preprint arXiv:1908.00016* (2019).
20. Skirlo, S. A., Lu, L. & Soljačić, M. Multimode one-way waveguides of large chern numbers. *Physical review letters* **113**, 113904 (2014).

21. Wheeler, W. A., Wagner, L. K. & Hughes, T. L. Many-body electric multipole operators in extended systems. *arXiv preprint arXiv:1812.06990* (2018).
22. Kang, B., Shiozaki, K. & Cho, G. Y. Many-body order parameters for multipoles in solids. *arXiv preprint arXiv:1812.06999* (2018).
23. Xie, B.-Y. *et al.* Second-order photonic topological insulator with corner states. *Physical Review B* **98**, 205147 (2018).
24. Benalcazar, W. A., Li, T. & Hughes, T. L. Quantization of fractional corner charge in n -symmetric higher-order topological crystalline insulators. *Physical Review B* **99**, 245151 (2019).
25. Noh, J. *et al.* Topological protection of photonic mid-gap defect modes. *Nature Photonics* **12**, 408 (2018).
26. Ni, X., Weiner, M., Alù, A. & Khanikaev, A. B. Observation of higher-order topological acoustic states protected by generalized chiral symmetry. *Nature materials* **18**, 113 (2019).
27. Zhang, X. *et al.* Second-order topology and multidimensional topological transitions in sonic crystals. *Nature Physics* **15**, 582 (2019).
28. El Hassan, A. *et al.* Corner states of light in photonic waveguides. *Nature Photonics* 1–4 (2019).
29. Chen, X.-D. *et al.* Direct observation of corner states in second-order topological photonic crystal slabs. *Physical Review Letters* **122**, 233902 (2019).

30. Schindler, F. *et al.* Higher-order topology in bismuth. *Nature physics* **14**, 918 (2018).
31. Xue, H., Yang, Y., Gao, F., Chong, Y. & Zhang, B. Acoustic higher-order topological insulator on a kagome lattice. *Nature materials* **18**, 108 (2019).

Acknowledgements This work was partly supported by the National Science Foundation through the University of Pennsylvania Materials Research Science and Engineering Center DMR-1720530 and grant DMR-1838412. L.H. was supported by the Air Force Office of Scientific Research under award number FA9550-18-1-0133. Work by ZA and EM on the symmetry analysis of the quadrupole phase was supported by the Department of Energy, Office of Basic Energy Sciences under grant DE FG02 84ER45118. B.Z. was supported by the Army Research Office under award contract W911NF-19-1-0087.

Author contributions L.H. and B.Z. conceived the idea. L.H. carried out numerical simulations. L.H., Z.A., E.M. and B.Z. discussed and interpreted the results. L.H and B.Z. wrote the paper with contribution from all authors. B.Z. supervised the project.

Competing Interests The authors declare no competing interests.

Correspondence Correspondence and requests for materials should be addressed to Bo Zhen. (email: bozhen@sas.upenn.edu).

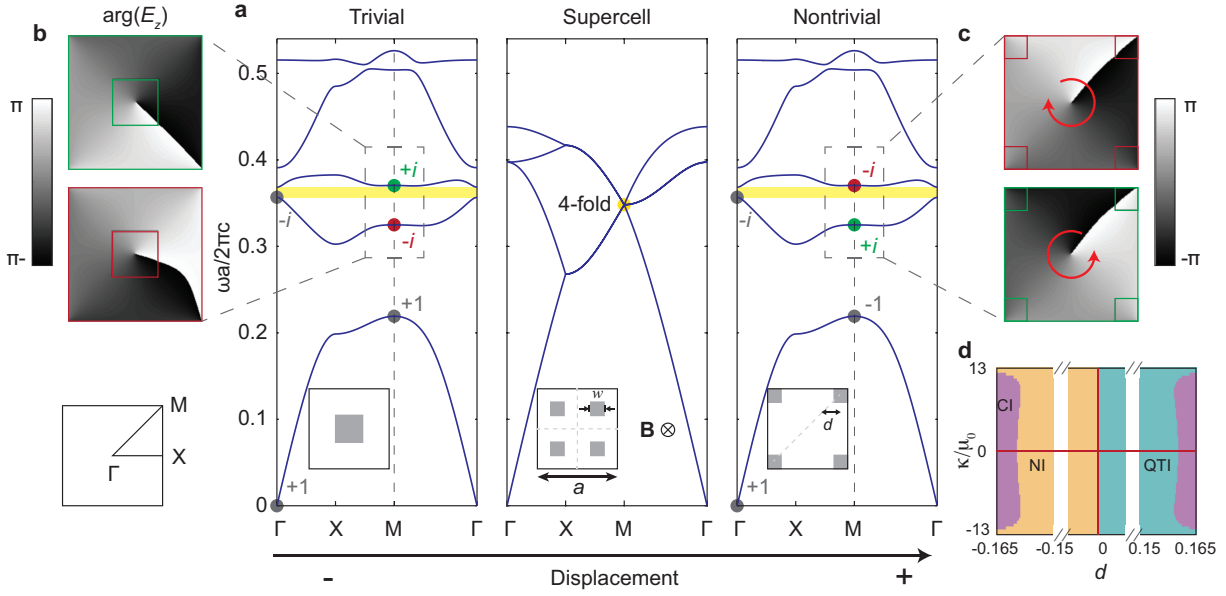


Figure 1: | **Quadrupole topological phase transitions through super-cell PhCs.** **a**, Band degeneracies are created at the center (Γ) and corner (M) of the folded Brilluion zone for a 2×2 super-cell PhC (inset). An external magnetic field (\mathbf{B}) induces gyromagnetic responses in YIG rods (gray squares), which breaks T but preserves C_4 . As the rods simultaneously move inward (left panel) or outward (right panel), the second gap is opened (shaded in yellow), but with different quadrupole phases: inward (outward) displacements with negative (positive) d correspond to trivial (nontrivial) quadrupole phases. The gyromagnetic response $\kappa = 12.4\mu_0$ is used in the calculations. **b,c** E_z mode profiles for the second and third modes at M feature a band inversion between the modes with C_4 index of $+i$ (green) and $-i$ (red) in the trivial and nontrivial phases. **d**, Complete topological phase diagram of the PhCs, including quadrupole phases (green), trivial phases (orange), and Chern insulating phases (purple). Systems are gapless along the axes (red). NI, normal insulator; QTI, quadrupole insulator; CI, Chern insulator.

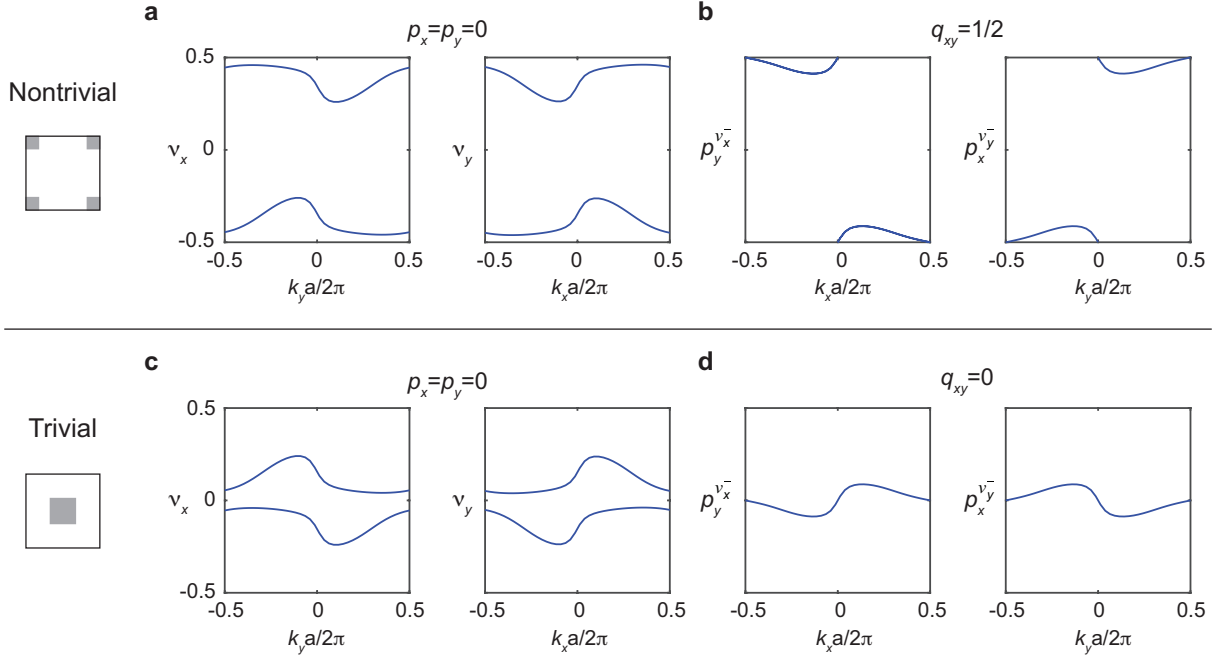


Figure 2: | **Confirmation of quadrupole and trivial PhCs through nested Wannier bands.** **a**, Wannier bands, $\nu_x(k_y)$ and $\nu_y(k_x)$, are calculated for the first and second bands of the quadrupole PhC. Results show the bulk dipole momentum is zero ($p_x = p_y = 0$). **b**, Calculations of the nested Wilson loops, $p_y^{\nu_x} = p_x^{\nu_y} = 0.5$, show the bulk quadrupole momentum q_{xy} is nontrivial and quantized to 0.5. **c,d** Similar calculations repeated for a trivial PhC, showing zero bulk dipole moments ($p_x = p_y = 0$) and zero quadrupole moments ($p_y^{\nu_x} = p_x^{\nu_y} = 0$).

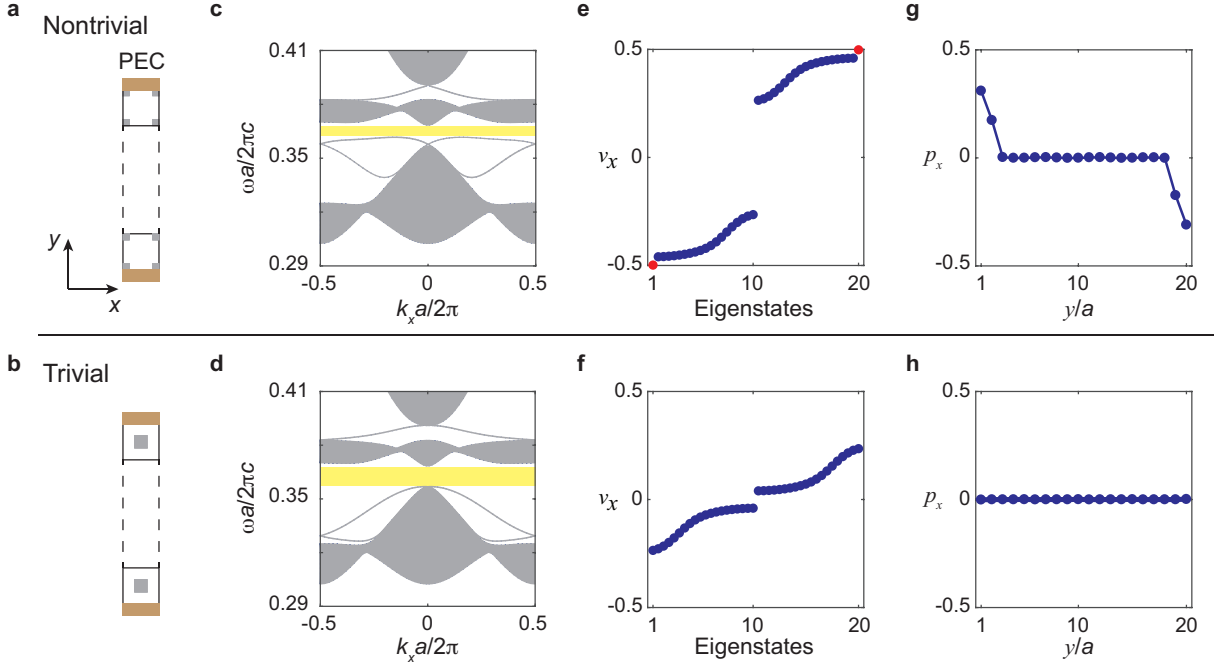


Figure 3: | **Physical consequences of quadrupole topological PhCs at 1D interfaces.** **a,b** Two 1D interfaces are created between a strip of quadrupole (trivial) PhC (same as Fig. 1a) and perfect electric conductors (PECs). **c,d** Energy dispersions of the two strip setups. **e**, For the nontrivial setup, Wannier centers of the eigenmodes show two Wannier states at ± 0.5 , which are outside the bulk Wannier bands due to the nontrivial bulk quadrupole moment. **f**, In comparison, no in-gap Wannier states are observed in the trivial setup. **g**, Calculation of the spatial density of polarization $p_x(y)$ shows the in-gap Wannier states are localized at the top ($y = 20a$) and bottom interfaces ($y = 0$). **h**, Similar calculations repeated for the trivial PhC, showing no edge polarization, which is consistent with the trivial quadrupole moment.

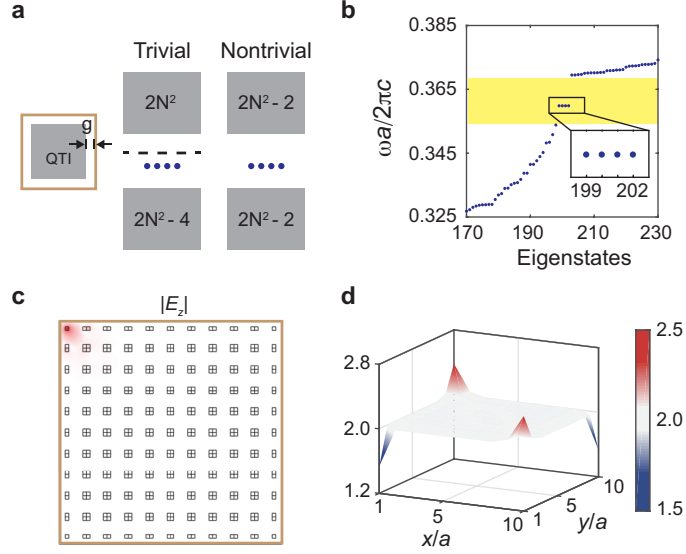


Figure 4: | **Topologically-protected corner states and filling anomaly in a 2D system.** **a**, For a finite PhC with $N \times N$ unit cells enclosed by PECs, the counting of the number of eigenstates below and above an energy gap are distinct between quadrupole and trivial phases. **b**, Eigenstates of a 10×10 quadrupole PhC, showing four degenerate corner states inside the bulk gap, shaded in yellow. **c**, Mode profile ($|E_z|$) of one of the corner states. **d**, Spatial distribution of the accumulative electromagnetic energy density for the lowest 200 energy eigenstates in the quadrupole PhC, showing fractional occupations (2 ± 0.5) at the corners.